RSC Advances

PAPER

View Article Online
View Journal | View Issue

Cite this: *RSC Adv.*, 2017, **7**, 42866

Low temperature annealing effects on martensitic transformation and exchange bias behavior of Ni–Mn–Sn free-standing alloy thin films

Zhenhua Wang,[a] Erjun Guo,[a] Changlong Tan,*[a] Xiaohua Tian,*[a] Wei Cai[b] and Jiachen Zhu[a]

Low temperature annealing (<500 °C) is the key to realizing the novel functionalities of Ni–Mn–Sn alloy thin film for applications in a micro-electro-mechanical systems (MEMS) drive. However, it is very difficult to realize the low temperature annealing of Ni–Mn–Sn thin films, which is limited due to substrate constraints. Herein we report the effects of low temperature annealing on the microstructure, martensitic transformation and exchange bias (EB) behavior of $Ni_{51}Mn_{36}Sn_{13}$ free-standing alloy thin films. We find that low temperature annealing significantly increases the degree of ordering in the austenite phase, leading to an increase in the martensitic transformation temperature (T_M) and the Curie temperature (T_C) of the austenitic phase. More interestingly, a narrow thermal hysteresis and exchange bias effects can be observed in the $Ni_{51}Mn_{36}Sn_{13}$ free-standing alloy thin films; EB field (H_E) and coercivity (H_C) increase with an increase in annealing temperature. When the annealing temperature of free-standing films is 673 K, the maximum H_E and H_C are 31.10 Oe and 129.64 Oe, respectively. Our work would enhance the material performance for low temperature annealing applications of Ni–Mn–Sn thin films in MEMS.

Received 19th July 2017
Accepted 20th August 2017

DOI: 10.1039/c7ra07942g

rsc.li/rsc-advances

1. Introduction

In recent years, Ni–Mn–Sn magnetic shape memory alloy thin films have attracted much attention, for applications such as in magnetic refrigerants, actuators, sensors, MEMS, *etc.*[1–5] As mentioned in previous reports, the Ni–Mn–Sn alloy thin films formed by magnetron sputtering system at room temperature are amorphous.[6–8] The amorphous thin films exhibit excellent shape memory effect after annealing, which makes them good candidates as material for MEMS devices. Therefore, appropriate annealing for a short time is necessary. Some researchers have studied the effects of substrate temperature and annealing treatment on the microstructure, martensitic transformation and magnetic properties of the Ni–Mn–Sn alloy thin films grown.[9–14] The results show that Ni–Mn–Sn alloy thin films were deposited on crystal substrates at substrate temperature above 500 °C, and annealing temperature is usually higher than 550 °C. As we know, a relatively high temperature is good for relieving accumulated strain energy, diminishing defects, and enlarging grain size to get obvious martensitic transformation and magnetic properties. However, the target composition and properties of Ni–Mn–Sn alloy thin films can be affected by high temperature annealing. This might lead to different microstructure, martensitic transformation and magnetic properties of Ni–Mn–Sn alloy thin films. Meanwhile, for microsensors technology, the temperature of some process has to be below the melting point of 500 °C.[15–17] Thus, low temperature annealing (<500 °C) may be a key approach to improve the applications of thin films in MEMS.

Unfortunately, very few reports focused on low temperature annealing effects on microstructure, martensitic transformation and magnetic properties of Ni–Mn–Sn alloy thin films. The low temperature annealing effects of the Ni–Mn–Sn thin films are limited due to the substrate constraints. This phenomenon occurs due to the elastic constraint set by the substrate, because of the lattice mismatch between the film and substrate.[18–21] When the thin films are heated or annealed, atoms need more energy to against with the internal stress between the substrate and thin films, through the grain boundary and the height of the energy barrier corresponding to the grain boundaries.[22,23] Thus, we suggest that the Ni–Mn–Sn free-standing alloy thin film could be annealed at a low temperature.[24] Moreover, the MEMS applications of Ni–Mn–Sn free-standing alloy thin film, such as microcantilever beam and micropumps are highlighted. Thus, the purpose of this study is to investigate the effect of low temperature annealing on martensitic transformation and magnetic properties of Ni–Mn–Sn free-standing alloy thin films. The results show that the low

[a]College of Materials Science and Engineering, Harbin University of Science and Technology, Harbin 150080, China. E-mail: changlongtan@hrbust.edu.cn; xiaohuatian@hrbust.edu.cn
[b]School of Materials Science and Engineering, Harbin Institute of Technology, Harbin 150001, China

temperature annealing not only significantly increases the degree of ordering in the austenite phase, but also increases both T_M and T_C of the austenitic phase. More interestingly, a narrow thermal hysteresis and EB effect of the $Ni_{51}Mn_{36}Sn_{13}$ free-standing alloy thin films is obtained, which makes them potential candidates for microelectromechanical systems (MEMS) applications.

2. Experimental

Fig. 1 shows a schematic of fabricating Ni–Mn–Sn free-standing alloy thin film. The photoresist thin film was deposited on silicon (100) substrate by spinning, and Ni–Mn–Sn thin film was deposited on photoresist/silicon substrate by dc magnetron sputtering system using $Ni_{50}Mn_{37}Sn_{13}$ (at%) sputtering target. The film was deposited on photoresist/silicon substrate under Ar gas pressure of 1.5×10^{-3} mbar using a DC power supply operating at 100 W for 2 hours, and the temperature of the substrate was 60 °C. Subsequently, the photoresist thin film was removed with acetone. Thickness of the Ni–Mn–Sn free-standing alloy thin film was measured with scanning electron microscope (SEM) and found to be 2.0 μm, the microstructure was studied using atomic force microscopy, and the film was annealed at 373, 473, 573 and 673 K for 1 hour each. The microstructure of the thin film was examined by atomic force microscopy, and the composition of the as-deposited films in austenite phase was determined by energy dispersive X-ray analysis is found to be $Ni_{51}Mn_{36}Sn_{13}$ (at%). The crystal structure at room temperature was determined by X-ray diffraction (XRD, Cu Kα radiation). The temperature dependence of magnetization $M(T)$ of the film was measured in an external magnetic field ($H = 100$ Oe), in the temperature range $5\ K \leq T \leq 400\ K$ using SQUID magnetometer (MPMS, Quantum Design) under zero field cooling (ZFC), field cooling (FC) and field heating (FH) modes. The measurements in the ZFC mode were taken by first cooling the film from 400 K to 5 K in the absence of the field and applying an external field of 100 Oe at low temperatures. The data were collected up to 400 K. The film was cooled down once again to 5 K, now in the presence of a field. Data were recorded in the FC mode and subsequently the film was heated in the presence of the field up to 400 K, and the measurements were taken in the FH modes. The magnetization hysteresis loops of the sample were measured at 5 K in a field ranging from 0.01 to 0.5T.

3. Results and discussion

Fig. 2 shows the XRD patterns of both the as-deposited and annealed Ni–Mn–Sn free-standing alloy thin films at room temperature. It is clear that the pattern of the as-deposited sample shows wide peaks with low intensities, and the as-deposited thin film displays a coexistence of amorphous, $L2_1$ cubic structure (austenite) as the A(220), A(222), A(422) peaks and a four-layered orthorhombic (4O) structure (martensite) as the 4O(023) peak.[25] The appearance of coexistence of an amorphous structure, a cubic structure and a 4O structure may be attributed to the partial crystallization of the as-deposited sample during the sputtering process. As demonstrated by the XRD profile, the patterns of annealed Ni–Mn–Sn free-standing alloy thin films can be indexed on the basis of a cubic single-phase austenite phase ($L2_1$), and the films exhibit nearly single phase with no detectable secondary or impurity phases.[26] Moreover, the relative intensity of all the peaks of annealed free-standing alloy thin films increases with increasing annealing temperature, and the relative intensity of peaks A(220) and A(422) enhances gradually, but that of the peak 4O(023) reduces.

In order to confirm the influence of annealing temperature on the composition, the composition of the films is determined by energy dispersive X-ray analysis. Analysis of the spectra after

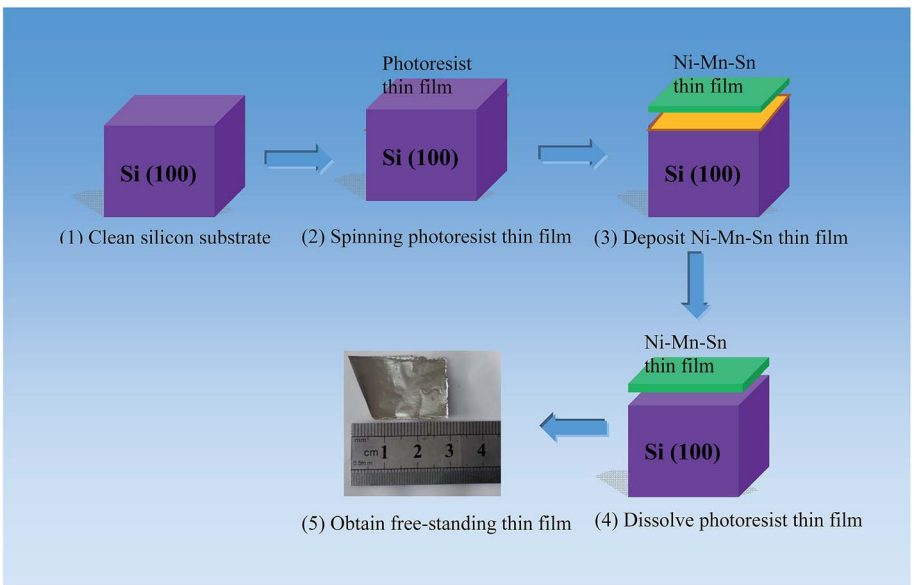

Fig. 1 Schematic of Ni–Mn–Sn free standing alloy thin film.

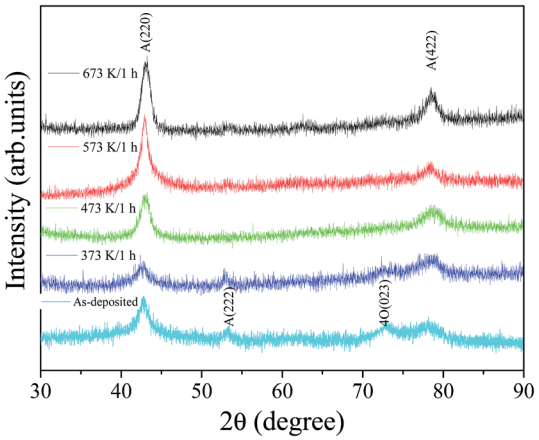

Fig. 2 XRD patterns of Ni–Mn–Sn free-standing alloy thin films in as-deposited state and low temperature annealing at 373 K, 473 K, 573 K, and 673 K for 1 hour, each.

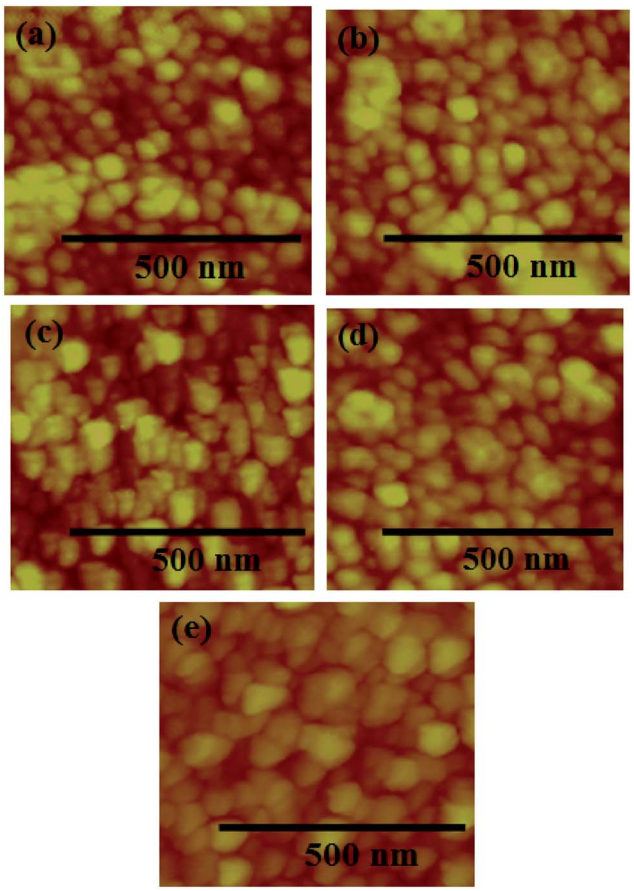

Fig. 3 AFM images for the surface morphology of Ni–Mn–Sn free-standing alloy thin films in as-deposited state and low temperature annealing at 373 K, 473 K, 573 K, and 673 K.

background subtraction and deconvolution of peaks confirm that the samples annealed at different temperatures have the same composition.

An analysis of the XRD pattern reveals that the lattice parameters of the free-standing alloy thin films in the as-deposited state and at annealing temperatures of 373, 473, 573, and 673 K are 5.890, and 5.906, 5.910, 5.919 and 5.924 Å, respectively. These values are close to those previously reported (5.925–5.972, 6.0 Å).[12,13,27] The summary of these lattice parameters and crystal structure is given in Table 1.

In order to further confirm the mean grain size in the films, the grain size of the $Ni_{51}Mn_{36}Sn_{13}$ free-standing thin films can be determined by the Scherrer's formula:[28]

$$D = k\lambda/\beta \cos\theta$$

where β is the FWHM of the peak, k is the constant, λ is the incident wavelength and θ is the diffraction angle. Thus, the grain size D of $Ni_{51}Mn_{36}Sn_{13}$ free-standing thin films can be calculated, and the average values of the grain size are given in Table 1.

According to Table 1, annealing temperatures from 373 to 673 K increase the grain size as a result of faster grain growth, which results in the reduction of grain boundaries that favour the formation of closed packed structure, leading to the development of strong (220) plane texture, consistent with the results of Fig. 2. However, the grain size and annealing temperature of $Ni_{51}Mn_{36}Sn_{13}$ free-standing thin films are relatively small.[13] The reason is that the crystallization activation energy of free-standing thin films is relatively low, *i.e.*, the thin films could still be crystallized, when the annealing temperature is below 500 °C. Furthermore, when the thin films are not been restrained by the substrate, the atoms do not need more energy to against with the internal stress between the substrate and thin films, through the grain boundary and the height of the energy barrier corresponding to the grain boundaries.

Table 1 Values of lattice parameter and grain size for the as-deposited thin films and different annealing temperatures of Ni–Mn–Sn free-standing alloy thin films

		Lattice parameter			Grain size (nm)	
	Annealing temperature (K)	a (Å)	b (Å)	c (Å)	XRD along (220) peak	Atomic force microscopy
Sample A	As-deposited	5.890	5.890	5.890	3.2	15.8
Sample B	373	5.906	5.906	5.906	4.1	21.9
Sample C	473	5.910	5.910	5.910	4.3	29.5
Sample D	573	5.919	5.919	5.919	7.2	45.3
Sample E	673	5.924	5.924	5.924	8.9	53.5

Therefore, the $Ni_{51}Mn_{36}Sn_{13}$ free-standing thin films can be annealed at low temperatures with a relatively small grain size.

In order to further confirm the grain size in Ni–Mn–Sn free-standing alloy thin films, atomic force microscopy was carried out. Fig. 3 shows the surface morphology of the as-deposited and annealed Ni–Mn–Sn free-standing alloy thin films. It is clear from the images that the grain size increases with an increase in the annealing temperature, which is in agreement with the XRD results. The values of grain size are reported in Table 1. An important point to be noted is that the overall grain size shown by atomic force microscopy was much bigger than that calculated by XRD, which is ascribed to the fact that atomic force microscopy shows agglomeration of the grain size whereas XRD gives an average mean grain size.[13] Thus, the XRD and

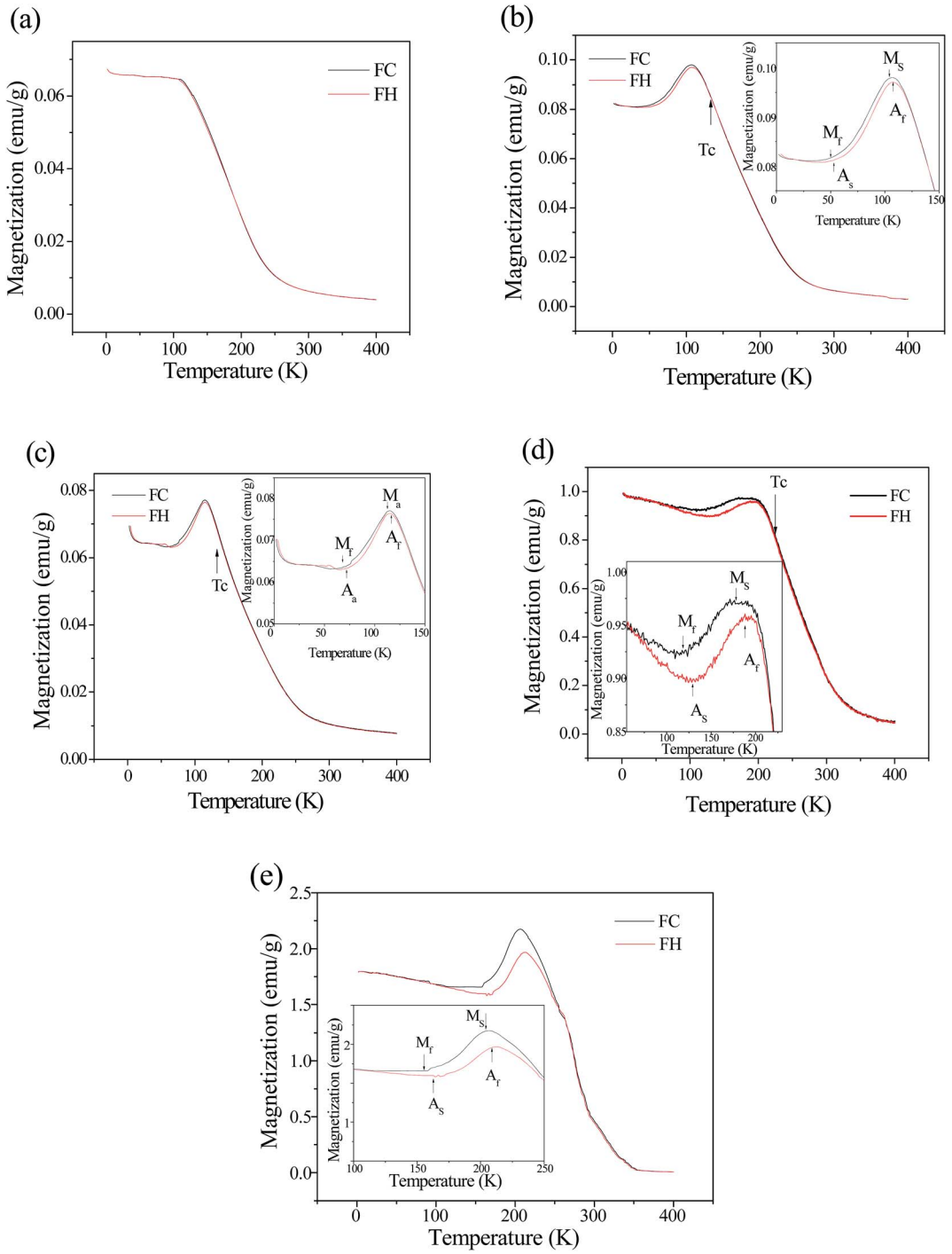

Fig. 4 The temperature dependence of magnetization in the as-deposited and annealed Ni–Mn–Sn free-standing alloy thin films in FC and FH modes from 5 K–400 K with a fixed magnetic field of 100 Oe. (a) As-deposited, (b) 373 K, (c) 473 K, (d) 573 K and (e) 673 K. Inset heating and cooling curves where phase transition occurs.

atomic force microscopy data can be in agreement with the grain growth. This result indicates that the effect of annealing on grain growth is obvious.

Fig. 4(a)–(e) shows the temperature dependence of magnetization in the as-deposited and annealed Ni–Mn–Sn free-standing alloy thin films in FC and FH modes from 5 K to 400 K with a fixed magnetic field of 100 Oe. As can be observed from Fig. 4(a), the magnetization increases continuously with a decrease in temperature from 260 to 160 K below which it remains constant. It is clear that the signature of phase transformation between martensite and austenite phase is not observed in the as-deposited film. The grain size of as-deposited films is only 3.2 nm. Moreover, the hysteresis between FC and FH curves characteristic of first-order phase transformation is also not present as the FH curve retraces the FC curve, which further confirms the absence of phase transformation. The absence of phase transformation could be due to the very small grain size in as-deposited film causing large number of grain boundary interfaces and associated excess free volume. Vishnoi *et al.*[13] indicate that the film-on-Si substrate of $Ni_{50}Mn_{35}Sn_{15}$ sputtering film cannot develop the martensitic transformation, when grain size of the film is smaller than 4.6 nm. The large number of grain boundaries, which act as potential barriers separating the individual grains, limits such type of atomic movements, impose constraints on the growth of the martensite structure and confine the transformed volume fraction in the nanocrystalline structure.

As observed from Fig. 4(b)–(e), all the low temperature annealing of Ni–Mn–Sn free-standing alloy thin films, upon temperature variation, undergo a change of magnetization typical for the first order martensitic transition and at higher temperatures a second order ferromagnetic–paramagnetic transition at Curie temperature of austenite, both of which are frequently observed in these systems. With the increase in annealing temperature, both T_M and T_C of the austenitic phase increase significantly, the values of measurement of which were reported in Table 2. Furthermore, the magnetization of annealed films increases with an increase in the annealing temperature, as shown in the inset of Fig. 4(b)–(e). Evidently, the low temperature annealing leads to an increase in the degree of order of associated excess free volume, and the number of grain boundary interfaces reduces gradually while the grain size of the annealed free-standing alloy thin films enhances. However, we found that the FC and FH curves, characteristic of first-order phase transformation, almost overlap each other, and the increase in magnetization is very low, as shown in the inset of Fig. 4(b) and (c). This phenomenon could be due to the nucleation and growth of crystallization process of Ni–Mn–Sn free-standing alloy thin film.[29,30] When the annealing temperature is below 473 K, the nucleation rate increases with the progress of annealing temperature, and Ni–Mn–Sn free-standing alloy thin film is transformed gradually from amorphous to crystalline. The atoms have more energy to overcome the activation energy barrier to nucleate at the beginning of the crystallization, and the degree of lattice order of films increases; however, the grain growth rate is relatively slow. Thus, the values of the grain size are relatively small, which are close to the grain size of the as-deposited film. Moreover, when the grain size is less than 4.3 nm, large amount of grain boundaries will promote the phase transformation since there are more defects, and the phase transformation is easier to occur there.[31,32] This would facilitate the martensitic transformation and the reverse transformation, resulting in a narrow thermal hysteresis, as shown in inset of Fig. 4(b) and (c).

From Fig. 4(d) and (e), the T_M and thermal hysteresis of annealed film increase with increase in annealing temperature. When the annealing temperature is 573 K, the characteristic temperatures of structural transition obtained from FC and FH curves are $M_s = 183.4$ K, $M_f = 123.5$ K, $A_s = 129.1$ K and $A_f = 190.1$ K, where M_s and M_f are martensite start and finish temperatures and A_s and A_f are austenite start and finish temperatures, respectively. In addition, it is evident that the grain size of free-standing film reaches 7.2 nm, and the thermal hysteresis of transformation is 6.7 K. This phenomenon could be due to the grain growth of Ni–Mn–Sn free-standing alloy thin films. It is well known that thermal hysteresis in martensitic transformation originates from frictional energy in the interfacial movement during the shear process. When the grain size of annealed films increases with increase in annealing temperature, martensitic transformation and reverse transformation will increase the movement distance and energy dissipation. Thus, the thermal hysteresis increases with increase in grain size, which is consistent with Tian's result.[33]

Fig. 5(a)–(e) show the temperature dependence of magnetization in ZFC and FC with 100 Oe applied field to characterize the magnetic transitions for Ni–Mn–Sn free-standing alloy thin films. From Fig. 5(a), the ZFC and FC curves split is not obvious with further decrease in temperature. It could be due to larger disorder in structure, which would affect the mobility of the twin boundaries.[34] However, with increase in annealing temperature, the ZFC and FC curves split, showing irreversible behaviour, and the splitting gets more enhanced with a decrease in temperature, as shown in the inset of Fig. 5(b)–(e). The splitting indicates the coexistence of antiferromagnetic (AFM) and ferromagnetic (FM) state exchange interaction in the film as reported for $Ni_{50}Mn_{50-x}Sn_x$ system.[35,36] As we all know, the AFM interaction in off-stoichiometric Ni–Mn–Sn is due to the AFM coupling between Mn atoms in the Mn sites and excess Mn atoms in the Sn sites.[37,38] This could be conducive to the

Table 2 Details of transformation temperatures obtained from magnetization *versus* temperature curves of as-deposited Ni–Mn–Sn free-standing alloy thin films and annealing temperatures ranging from 373 K to 673 K

	Transition temperatures (K)				Curie temperature (K)	Hysteresis width (K)
	M_s	M_f	A_s	A_f		
Sample A	—	—	—	—	—	—
Sample B	104.9	53.9	57.2	108.1	127	3.2
Sample C	112.6	70.4	73.9	116.3	143	3.7
Sample D	183.4	123.5	129.1	190.1	210	6.7
Sample E	205.7	157.9	165.8	213.4	260	7.9

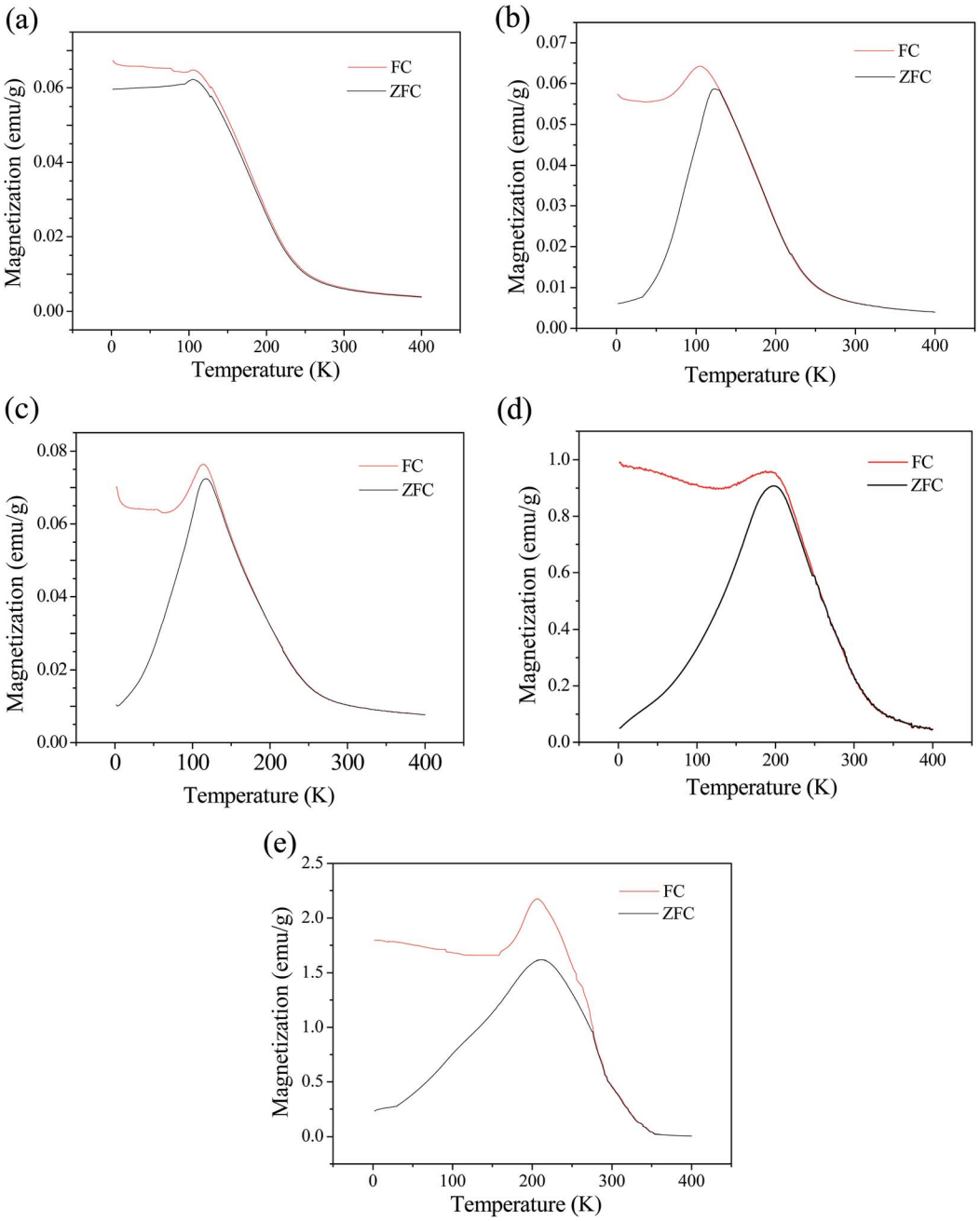

Fig. 5 Temperature dependent magnetization after ZFC and FC of the as-deposited and annealed Ni–Mn–Sn free-standing alloy thin films under a magnetic field of 100 Oe. (a) As-deposited, (b) 373 K, (c) 473 K, (d) 573 K and (e) 673 K.

formation of a closed packed structure, which leads to increase in degree of AFM lattice order.

In order to confirm the occurrence of EB effect in our film, we measured magnetization hysteresis loops at $T = 5$ K and the low field range from -0.5 to $0.5T$, shown in Fig. 6. The EB field (H_E) and coercivity (H_C) are calculated using $H_E = -(H_1 + H_2)/2$ and $H_C = |H_1 - H_2|/2$, where H_1 and H_2 are the left and right coercive fields at which the magnetization equals to zero, respectively. The values of H_E and H_C are reported in Table 3. It can be seen that the EB properties were found to be different in the as-deposited and low temperature annealed films. Inset of Fig. 6(b)–(e) clearly shows the magnified view of loop shift towards the negative field axis and a more pronounced shift at 5 K. This provides evidence of the existence of EB effect in these annealing films. Furthermore, the values of H_E and H_C increase with increase in annealing temperature. It can be explained by the unidirectional anisotropy produced by the AFM–FM coupling at the interface of two coupled phases.[34,36] Increase in annealing temperature from 373 to 673 K increases grain size as a result of faster grain growth, which results in reduction of grain boundaries that favour the formation of closed packed structure, leading to an increase in the degree of AFM lattice

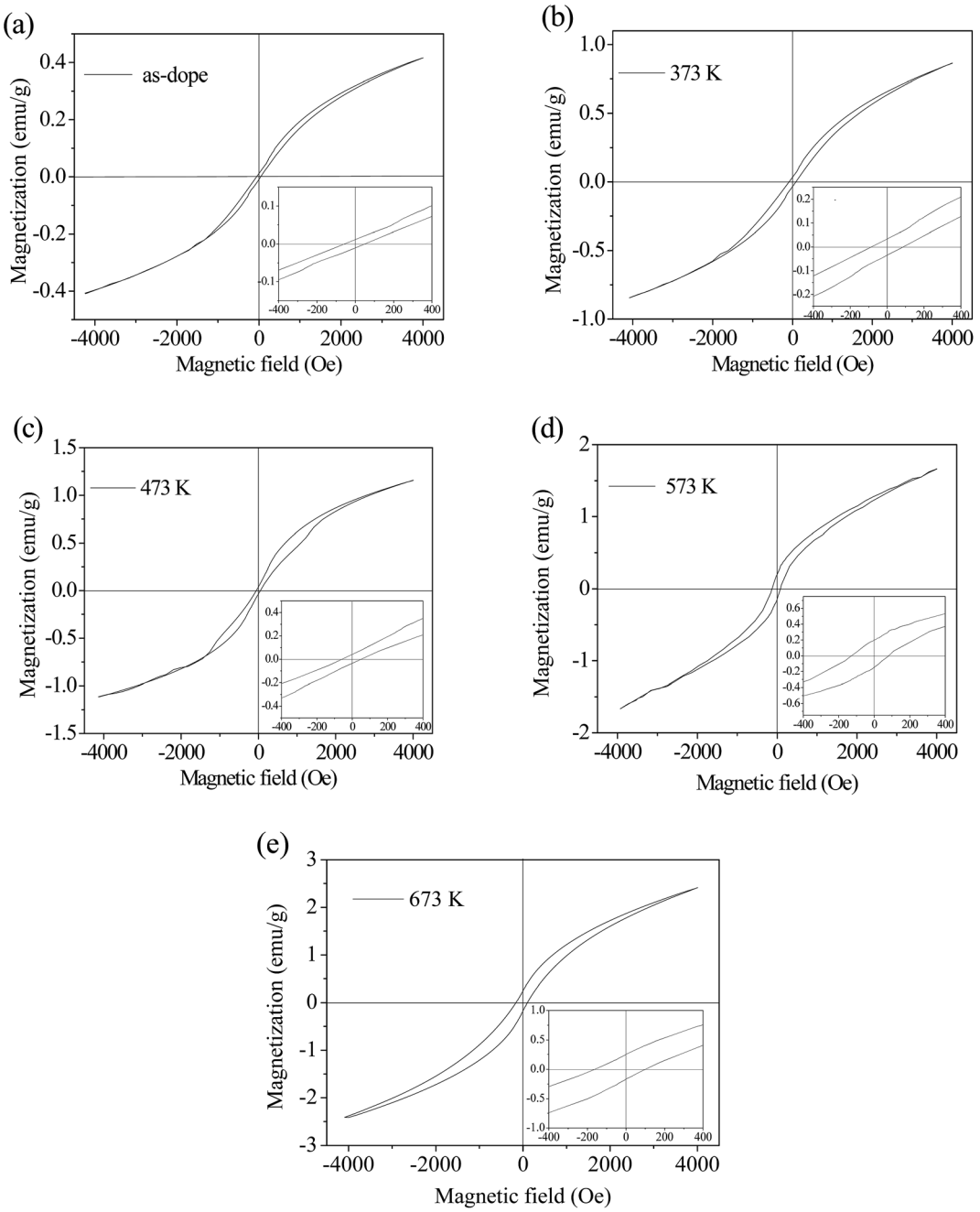

Fig. 6 Magnetization hysteresis loops of Ni–Mn–Sn free-standing alloy thin films (a) as-deposited, (b) 373 K, (c) 473 K, (d) 573 K and (e) 673 K measured at 5 K. The insets show an enlarged view of the central region of the loops.

Table 3 Detailed values of H_c and H_E of the as-deposited Ni–Mn–Sn free-standing alloy thin films and annealing temperatures ranging from 373 K to 673 K, measured at 5 K

	Annealing temperature (K)	Exchange bias field H_E (Oe)	Coercivity H_c (Oe)
Sample A	As-deposited	—	65.41
Sample B	373	1.10	66.21
Sample C	473	14.45	65.81
Sample D	573	27.40	102.41
Sample E	673	31.10	129.64

order. The unidirectional anisotropy produced by the AFM increases with an increase in low temperature annealing. When the low cooling field is constant, the intensity of the AFM–FM coupling increases with increase in unidirectional anisotropy produced by the AFM. However, we find that the EB effect is not observed in the as-deposited free-standing films, as shown in the inset of Fig. 6(a). This phenomenon could be due to the absence of martensite. According to Fig. 4(a), there is no martensite (which is the phase that exhibits EB) present in this film. The corresponding variations of H_E and H_C are shown in Fig. 7. It is evident that both H_E and H_C increase with increase in

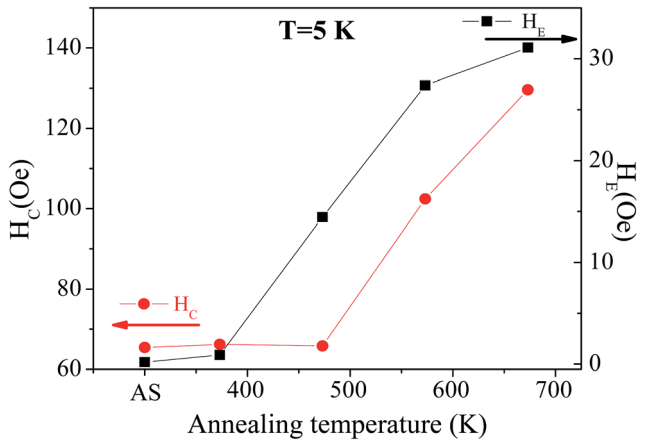

Fig. 7 The variation of EB field (H_E) and coercivity (H_C) with temperature.

annealing temperature. When the annealed temperature of free-standing films is 673 K, the maximum H_E and H_C are 31.10 Oe and 129.64 Oe, respectively. The increase in H_E and H_C could be attributed to the increase in AFM order with annealed temperature. AFM–FM coupling increases with increase in unidirectional anisotropy produced by the AFM.

4. Conclusions

In conclusion, we have observed the effects of low temperature annealing on microstructure, martensitic transformation and EB effect of $Ni_{51}Mn_{36}Sn_{13}$ free-standing alloy thin films. We found that the as-deposited thin film displays a coexistence of amorphous and $L2_1$ cubic structure (austenite) structure. Moreover, the martensite transformation and EB effect were not observed in the as-deposited thin film. For the low temperature annealed films, the patterns of annealed free-standing thin films could be indexed on the basis of a cubic single-phase austenite phase ($L2_1$). The grain size, martensitic transformation and exchange bias (EB) effect of free-standing thin films were significantly affected by low temperature annealing. With increase in annealing temperature, the grain size of free-standing films increased from 3.2 to 8.9 nm, and the T_M of free-standing films were 104.9, 112.6, 183.4, 205.7 K. More interestingly, we found that a narrow thermal hysteresis was obtained in the $Ni_{51}Mn_{36}Sn_{13}$ free-standing alloy thin films, which could be due to the grain size effect and order degree of films at annealing temperature. At an annealing temperature of 373 K, the thermal hysteresis of transformation was only 3.2 K. Moreover, EB behaviour was observed in $Ni_{51}Mn_{36}Sn_{13}$ free-standing alloy thin films, and we believe that this is attributed to the unidirectional anisotropy, which arose due to the coupling of AFM and FM interactions in the martensite phase of the film.

Conflicts of interest

There are no conflicts to declare.

Acknowledgements

The authors acknowledge the support from the National Natural Science Foundation of China (Grant No. 51471064 and 51301054); the Program for New Century Excellent Talents (Grant No. 1253-NCET-009); and Program for Youth Academic Backbone in Heilongjiang Provincial University (Grant No. 1251G022).

References

1 Y. Sutou, Y. Imano, N. Koeda, T. Omori, R. Kainuma, K. Ishida and K. Oikawa, *Appl. Phys. Lett.*, 2004, **85**, 4358.
2 N. Teichert, A. Auge, E. Yüzüak, I. Dincer, Y. Elerman, B. Krumme, H. Wende, O. Yildirim, K. Potzger and A. Hüzütten, *Acta Mater.*, 2015, **86**, 279–285.
3 R. Modak, B. Samantaray, P. Mandal and A. Srinivasan, *Appl. Phys. A*, 2016, **122**, 252.
4 K. Ullakko, J. K. Huang, C. Kantner, R. C. O'Handley and V. V. Kokorin, *Appl. Phys. Lett.*, 1996, **69**, 1966–1968.
5 S. J. Murray, M. Marioni, P. G. Tello, S. M. Allen and R. C. O'Handley, *J. Magn. Magn. Mater.*, 2009, **945**, 226–230.
6 R. Modak, B. Samantaray, P. Mandal and A. Srinivasan, *J. Alloys Compd.*, 2017, **692**, 529–534.
7 M. Rajkumar, B. Deka, R. M. Manivel and A. Srinivasan, *Adv. Sci. Lett.*, 2016, **22**, 26–29.
8 R. Vishnoi, R. Singhal and D. Kaur, *J. Nanopart. Res.*, 2011, **13**, 3975–3990.
9 R. Vishnoi and D. Kaur, *Surf. Coat. Technol.*, 2010, **204**, 3773.
10 E. Yüzüak, I. Dincer, Y. Elerman, A. Auge, N. Teichert and A. Hütten, *Appl. Phys. Lett.*, 2013, **103**, 222403.
11 A. Auge, N. Teichert, M. Meinert, G. Reiss, A. Hütten, E. Yüzüak, I. Dincer, Y. Elerman, I. Ennen and P. Schattschneider, *Phys. Rev. B: Condens. Matter Mater. Phys.*, 2012, **85**, 214118.
12 R. Vishnoi and D. Kaur, *J. Alloys Compd.*, 2011, **509**, 2833.
13 R. Vishnoi and D. Kaur, *Surf. Coat. Technol.*, 2010, **204**, 3773–3782.
14 L. Larson and K. Johnson, *IEEE Electronic Components and Technology Conf*, ECTC, Las Vegas, NV, June 1–3, 2016, pp. 1952–1957.
15 C. T. Pan, H. Yang, S. C. Shen, M. C. Chou, H. P. Chou, R. Vishnoi and D. Kaur, *J. Micromech. Microeng.*, 2002, **12**, 611.
16 A. Shah, M. Mayer, Y. Zhou, S. J. Hong and J. T. Moon, *Microelectron. Eng.*, 2008, **85**, 1851.
17 J. R. Ho, C. C. Chen and C. H. Wang, *Sens. Actuators, A*, 2004, **111**, 188.
18 A. Hakola, O. Heczko, A. Jaatinen, V. Kekkonen and T. Kajava, *J. Phys.: Conf. Ser.*, 2007, **59**, 122–125.
19 Y. L. Li, S. Y. Hu, Z. K. Liu and L. Q. Chen, *Acta Mater.*, 2002, **50**, 395–411.
20 W. Lu and D. Kim, *Appl. Phys. Lett.*, 2006, **88**, 153116.
21 L. W. Brownlow and C. H. Wilts, *J. Appl. Phys.*, 1970, **41**, 1250.
22 A. Behler, N. Teichert, B. Dutta, A. Waske, T. Hickel, A. Auge, A. Hütten and J. Eckert, *AIP Adv.*, 2016, **3**, 122112.

23 R. Machavarapu and G. Jakob, *Appl. Phys. Lett.*, 2013, **102**, 232406.
24 Z. H. Wang, E. J. Guo, C. L. Tan and X. H. Tian, *Vacuum*, 2016, **130**, 124–129.
25 H. X. Zheng, W. Wang, S. C. Xue, Q. J. Zhai, J. Frenzel and Z. P. Luo, *Acta Mater.*, 2013, **61**, 4648.
26 H. X. Zheng, W. Wang, D. Z. Wu, S. C. Xue, Q. J. Zhai, J. Frenzel and Z. P. Luo, *Intermetallics*, 2013, **36**, 90.
27 J. Dubowik, I. Gościańska, Y. V. Kudryavtsev and A. Szlaferek, *J. Magn. Magn. Mater.*, 2007, **310**, 2773–2775.
28 B. D. Cullity, *Elements of X-ray Diffraction*, Addison-Wesley, Reading, M. A, 1970, p. 102.
29 Z. Z. Yuan, X. D. Chen, B. X. Wang and Z. J. Chen, *J. Alloys Compd.*, 2005, **399**, 166.
30 J. Malek, *Thermochim. Acta*, 1995, **267**, 60–73.
31 A. Talis and V. Kraposhin, *Acta Crystallogr., Sect. A: Found. Adv.*, 2014, **70**, 616.
32 K. Li, Y. Li, K. Y. Yu, C. Liu, D. Gibson, A. Matthews and Y. Q. FU, *Appl. Phys. Lett.*, 2016, **108**, 171907.
33 X. H. Tiana, J. H. Sui, X. Zhang, X. H. Zheng and W. Cai, *J. Alloys Compd.*, 2012, **514**, 210.
34 R. Vishnoi and D. Kaur, *J. Alloys Compd.*, 2011, **509**, 2833–2837.
35 T. Krenke, M. Acet, E. F. Wassermann, X. Moya, L. Mañosa and A. Planes, *Phys. Rev. B: Condens. Matter Mater. Phys.*, 2005, **72**, 014412.
36 R. Machavarapu and G. Jakob, *Appl. Phys. Lett.*, 2013, **102**, 232406.
37 C. V. Stager and C. C. M. Campbell, *Can. J. Phys.*, 2004, **56**, 1978.
38 A. Behler, N. Teichert, B. Dutta, A. Waske, T. Hickel, A. Auge, A. Hütten and J. Eckert, *AIP Adv.*, 2013, **3**, 122112.